Assembly Process and Electrical Properties of Top-Transferred Graphene on Carbon Nanotubes for Carbon-Based Three-Dimensional Interconnects

Ye Zhu, Chong Wei Tan, Shen Lin Chua, Yu Dian Lim, Boris Vaisband, Beng Kang Tay, *Member, IEEE*, Eby G. Friedman, *Fellow, IEEE*, Chuan Seng Tan, *Senior Member, IEEE*

***Abstract*—Carbon nanomaterials, graphene and carbon nanotubes (CNTs) have emerged as the promising materials for the integration of future advance packaging technologies. The main benefits of carbon nanomaterials include excellent electrical, thermal and mechanical properties. In this work, transfer process of a top graphene layer onto the as-grown carbon nanotube (CNT) bundles was successfully performed with direct graphene-to-CNT contact at the interface. Four-point-probe (4PP) I-V characterization suggests that an ohmic contact was achieved between the graphene and CNTs. Low CNT bump resistance of 2.1Ω for 90,000 μm^2 CNT area including the CNT/graphene contact resistance was obtained, demonstrating reduction of contact resistance between CNT and Au under the same fabrication and measurement conditions. This work presents the preliminary results for the assembly process of top-transferred graphene on CNTs and the electrical properties of direct CNT/graphene contact, paving the way for the implementation of full carbon-based three-dimensional (3D) interconnects.**

***Index Terms*—Carbon nanotube (CNT), Graphene, Three-dimensional (3D) interconnects**

I. Introduction

THE continuous miniaturization of integrated circuits (ICs) as driven by Moore's Law result in progressive performance improvement and cost reduction in electronic products over the past 40 years [1]. In recent years, however, this progressive trend has been constrained as the device scaling reaches the fundamental physical limitations. The escalating cost of Moore's Law has pivoted the semiconductor industry's focus to "More-than-Moore (MtM)" technologies [2]. Supported by advanced packaging solutions, high-density heterogeneous integration of analog/mixed-signal, RF, MEMS and image sensing with CMOS in a variety of 2.5D and 3D architectures is expected the main driving forces for the next-generation electronic products [3].

This work was supported by MOE Tier-2 grant #MOE2014-T2-2-105 (ARC22/15).

Ye Zhu, Chong Wei Tan, Shen Lin Chua, Yu Dian Lim, Beng Kang Tay and Chuan Seng Tan are with the School of Electrical and Electronic Engineering, Nanyang Technological University, NOVITAS, 50 Nanyang Avenue, 639798, Singapore (e-mail: Ye Zhu: yzhu012@e.ntu.edu.sg; Chuan Seng Tan: TanCS@ntu.edu.sg).

Boris Vaisband is with the Department of Electrical and Computer Engineering, University of California, Los Angeles, CA 90095, USA

Eby G. Friedman is with the Department of Electrical and Computer Engineering, University of Rochester, Rochester, NY 14627, USA

Vertical stacking of IC layers to form three-dimensional (3D) integration is one of the recent focuses in the advanced electronic packaging techniques [4], [5]. Apart from higher integration density obtained by 3D stacking, it can also achieve a complete functional unit by system-in-package integration. To realize this, reliable and efficient electrical interconnects for signal transmission and power distribution are needed [6]. Among the signal transmission techniques, flip chip bump and through-silicon via (TSV) technologies have been used for the vertical interconnections between chip and substrate. Flip chip bumps are able to achieve higher input/output (I/O) counts due to short electrical connection paths [7]; whereas TSV technology enables faster, short-path communication channeling between the vertically stacked ICs and devices [8].

A technical challenge in existing flip chip bumps and TSVs is the difference in coefficient of thermal expansion (CTE) between copper bump/TSV-filler and its surrounding materials. Due to the relatively large CTE mismatch between silicon (2.3×10^{-6}/°C) and copper (17×10^{-6}/°C) [9], [10], Cu-based pillar bumps and TSVs fabricated on Si substrate arises numerous stability and reliability issues during chip operation, especially in fluctuated temperature conditions.

Carbon nanomaterials, graphene and carbon nanotubes (CNTs) have emerged as promising materials for the integration in the next-generation advanced packaging technologies [11], [12]. The main benefit of carbon nanomaterials, e.g. CNTs, lies in their excellent electrical, thermal and mechanical properties: (i) low electrical resistivity, measured in a range of 0.8~33.8 mΩ •cm for single CNT and CNT bundles [13]–[15]; (ii) high current density ~10^9 A/cm^2 in single CNT [16]; (iii) high thermal conductivity, reported in a range of 600-3,000 W/mK for individual multi-walled carbon nanotubes (MWCNTs) [17]–[20]; and (iv) closer CTE to Si (2.3×10^{-6}/°C) as compared to Cu (17×10^{-6}/°C), e.g. ~2×10^{-6}/°C for single-walled carbon nanotubes (SWCNTs) [21]. At the same time, the porous structure of CNT bundles eases the thermal mismatch stress introduced in the surrounding Si substrate [9]. These advantages enable carbon nanomaterials to be highly attractive candidates as both on-chip and off-chip interconnects in 3D integration. Currently, substantial works have been done for the fabrication and characterization of CNT TSVs on conductive metal lines [22], [23]. Meanwhile, CNT bumps have been demonstrated as the potential flip chip bumps by several groups [24]–[26]. Apart from CNTs, graphene has

This article has been accepted for publication in a future issue of this journal, but has not been fully edited. Content may change prior to final publication. Citation information: DOI 10.1109/TCPMT.2019.2940511, IEEE Transactions on Components, Packaging and Manufacturing Technology

also been proposed as a potential candidate to replace copper as the next-generation planar interconnects due to its patterning feasibility and high current mobility [27]–[30].

Besides the thermal mismatch issue, full carbon-based interconnects are expected to have better out-of-plane and in-plane electrical properties as compared to their copper counterparts [31]. It has been demonstrated that the full integration of intercalation-doped multi-layer graphene (MLG) wires and CNTs offers better electrical performance reliability as compared to the Cu interconnects at 5nm node [32]. Another successful fabrication of graphene-CNT heterostructure for the off-chip interconnects has been made through a direct growth of CNTs within the vias, on top of the graphene [33]. To form a complete bottom-up full-carbon 3D interconnection, assembly process of the top graphene layer after the CNT growth needs be explored. Meanwhile, electrical properties of the contact formed between CNTs and top graphene layer after the assembly process requires further investigations.

In this work, we have successfully performed an assembly process by transferring a top layer of graphene onto the as-grown CNTs with direct graphene-to-CNT contact at the interface. The electrical properties of CNT/graphene contact was characterized by four-point-probe (4PP) I-V measurements of an Au-CNT-graphene-CNT-Au structure. The CNT/graphene contact resistance was benchmarked against the value of CNT/Au under the same fabrication and measurement conditions.

II. Experimental Methods

Major fabrication and assembly steps of the Au-CNT-graphene-CNT-Au structure are summarized in Fig. 1. The fabrication uses Si substrate with 280 nm SiO_2 layer deposited using thermal oxidation technique (Fig. 1, step 1). First, bottom Au pads (20nm Ti/100nm Au) and buffer/catalyst layer (8nm Al/2nm Al_2O_3/1.1nm Fe) were sequentially patterned on a silicon wafer using e-beam evaporation deposition and lift-off process (Fig. 1, step 2). Then, free-standing CNTs were grown using thermal chemical vapour deposition (TCVD) method with hydrogen (H_2) and acetylene (C_2H_2) gas flow ratio of 3:1 at 650˚C (Fig. 1, step 3). After CNT growth, two pieces of 80μm thickness polyethylene terephthalate (PET) with double-side non-conducting adhesives were assembled on the sides of CNT bundles as the spacers to support the free-standing CNTs when the top graphene layer was transferred (Fig. 1, step 4). Finally, few-layer graphene on PET (or SiO_2/Si) substrate was flipped over and pressed down onto the CNT bundles (Fig. 1, step 5 and 6). Graphene with the substrate was attached by the mechanical force of the top adhesive of PET spacers, creating direct contact between the graphene and CNTs.

The high contact resistance between CNTs and metal is always a key issue in CNT interconnects limiting their feasibility in the application [6], [22]–[24], [33]–[37] However, significant discrepancies are present in the state-of-the-art values of CNT/metal contact resistance, due to the absence of standardized techniques for CNT resistance. In our work, Au film (on SiO_2/Si substrate) is used as the control sample under identical CNT growth conditions and assembly processes. Four-point-probe (4PP) I-V measurements were used to characterize the electrical properties of the graphene and Au bridge structure. The total resistance of the graphene and Au bridge structure can be expressed as:

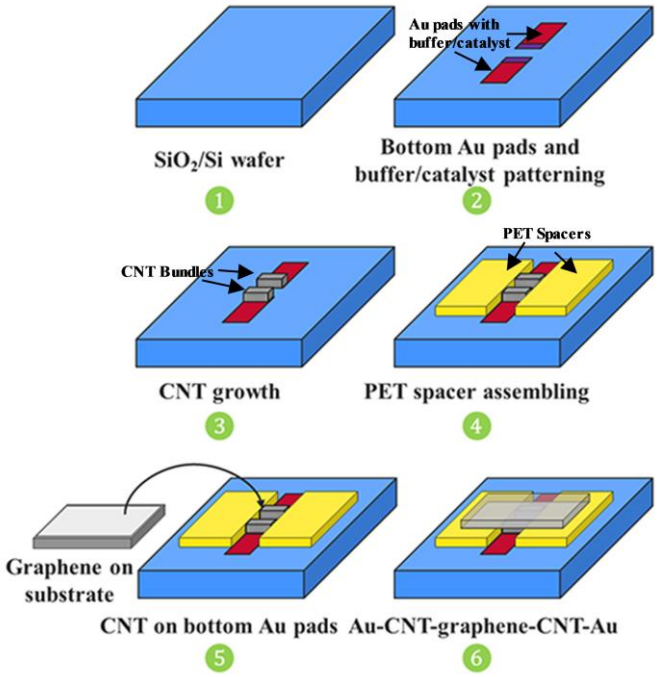

Fig. 1. Fabrication and assembly steps of the Au-CNT-graphene-CNT-Au structure.

$$R_{total} = R_{btm\_Au} + 2R_{Au-CNT-G} + R_G \quad (1)$$

and

$$R_{total} = R_{btm\_Au} + 2R_{Au-CNT-Au} + R_{top\_Au} \quad (2),$$

correspondingly, where R_{btm_Au} is the resistance of bottom Au pads; $R_{Au-CNT-G}$ and $R_{Au-CNT-Au}$ are the resistance of one CNT bump including the contact resistance of CNT/bottom Au, the resistance of bulk CNT and the contact resistance of CNT/graphene or CNT/top Au; R_G and R_{top_Au} are the resistance of top graphene layer and Au film, respectively. Eq. (1) and (2) is established based on the assumption where Au, CNTs, and graphene exhibit similar behavior has Ohmic resistors, connecting in series during electrical conduction.

To extract the $R_{Au-CNT-G}$ and $R_{Au-CNT-Au}$ in (1) and (2), the values of R_{btm_Au}, R_G and R_{top_Au} need to be determined. R_{btm_Au} can be measured from the control groups with the same dimension of bottom Au pads. R_G and R_{top_Au} can be estimated using the equation of $R = \frac{L}{W_{eff}} R_S$ (3), where L is the distance between two CNT bundles; W_{eff} is the effective width of top graphene layer or Au film; R_S is the sheet resistance of the graphene layer or Au film. Nevertheless, to utilize Eq. (1) and (2), CNT resistance needs to be subtracted. Using the reported CNT resistivity of 9.7 to 33.8 mΩ•cm [6], [15], CNT resistance can be determined using Ohm's law. However, the calculation is carried out based on the assumptions where the current density distribution and the crystallinity across the whole CNT bundles is similar. In actual CNT growth,

This article has been accepted for publication in a future issue of this journal, but has not been fully edited. Content may change prior to final publication. Citation information: DOI 10.1109/TCPMT.2019.2940511, IEEE Transactions on Components, Packaging and Manufacturing Technology

discrepancies in crystallinity and current density across various regions of CNT bundles can be anticipated. Nevertheless, in this work, the overall electrical properties of CNT bundles is taken into consideration to explore the feasibility of CNT-graphene heterostructure in TSV interconnect applications.

III. Results and Discussion

Graphene substrates used in this work were intrinsic CVD graphene transferred on the top of PET (or 350nm SiO_2/Si wafer) with a dimension of 10mm × 10mm. The structural characteristics of graphene were confirmed by optical microscopy and Raman characterization as 1-3 layers poly-crystal graphene (Fig. 2). On the other hand, 20nm

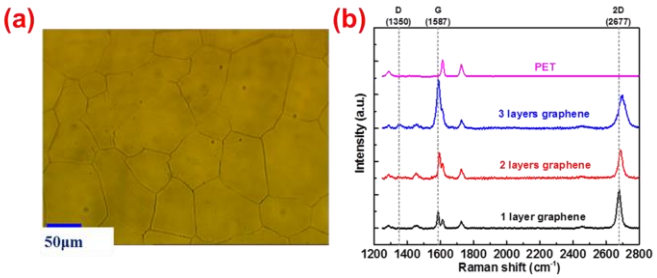

Fig. 2. (a) Optical and (b) Raman images of the graphene on SiO_2/Si and PET.

Ti/100nm Au was deposited by e-beam evaporation on 280nm SiO_2/Si wafer to be used as the control samples compared to the graphene samples. The sheet resistances of graphene layer and Au film were 218-237 and 0.31-0.32 Ω/sq, respectively, measured by 4PP sheet resistance measurement system. High sheet resistance of graphene may be attributed to the grain boundaries of poly crystal formed during the CVD growth,

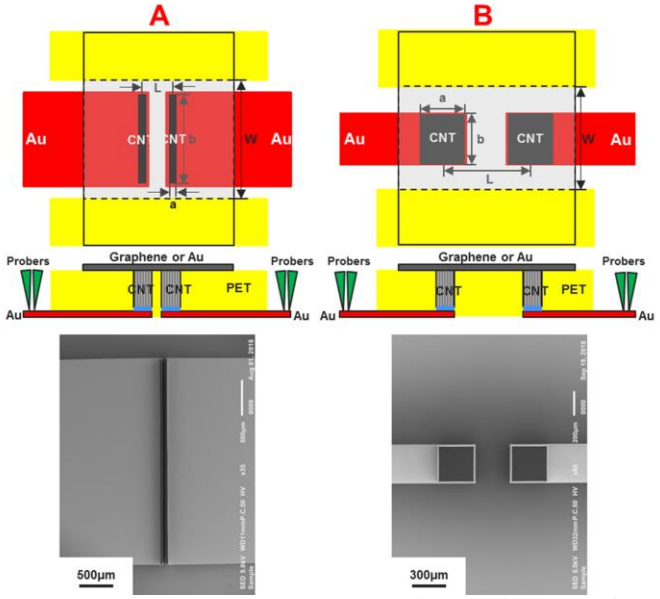

Fig. 3. Schematic diagrams and SEM images of two configurations of CNT area with the same size (left: configuration A, right: configuration B).

whereas the observed defects could be induced during the transferring process of micro-scale area onto the substrate.

Based on (3), R_G will be ~730 times larger than R_{top_Au} with the same dimension (L/W_{eff}), leading to a significant increase of the total resistance of the graphene bridge structure. To reduce the effect of R_G, another configuration of CNT area (Fig. 3, configuration A) with much smaller distance (L) between two CNT bundles was designed to benchmark against the regular square-shaped CNT area (Fig. 3, configuration B). The

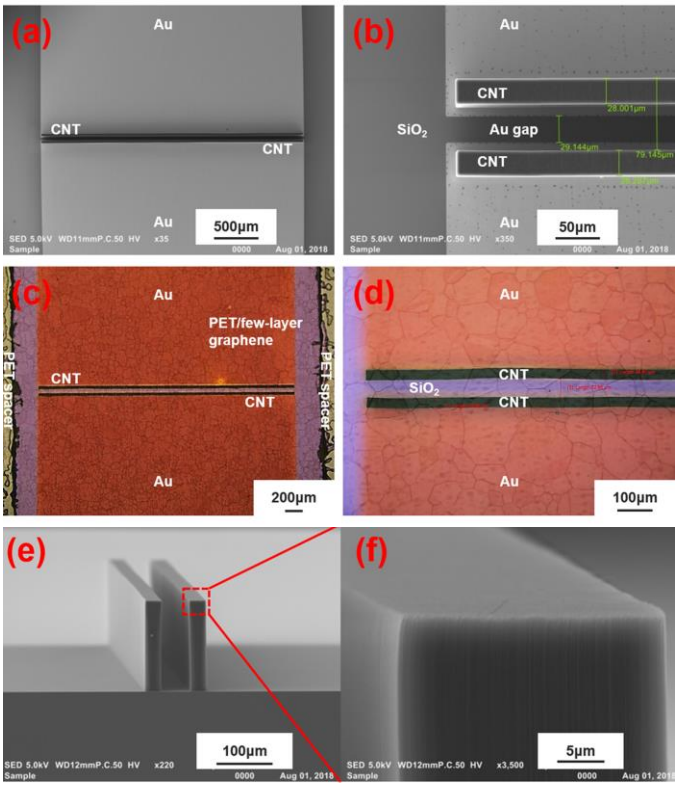

Fig. 4. (a) and (b) SEM images after CNT growth; (c) and (d) optical images after top graphene layer transferred; (e) and (f) SEM cross-section view of two CNT walls of the dummy sample cut in half.

size of CNT area in configuration A and B was maintained at the same value.

Optical microscopy and scanning electron microscopy (SEM) images of the fabricated Au-CNT-graphene-CNT-Au structure of configuration A are presented in Fig. 4. As shown in Fig. 4 (a) and (b), two CNT walls grown on top of the bottom Au pads

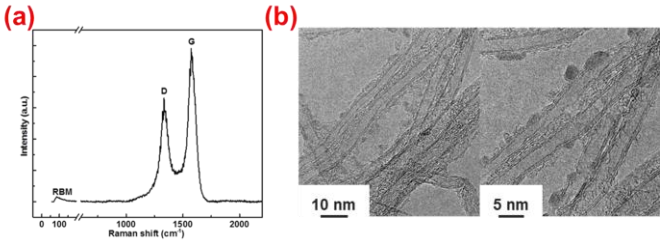

Fig. 5. (a) Raman and (b) transmission electron microscopy (TEM) images of the as-grown CNTs.

were uniform and well-aligned. Fig. 4 (c) and (d) show the direct contact of poly-crystal graphene with observable grain boundaries to the CNTs. Meanwhile, SEM image of the cross-section view of the two CNT walls is shown in Fig. 4 (e) and (f). The vertical length of CNTs was fine-tuned to be slightly higher than the thickness of the PET spacers (80 μm). Here, the vertical length of CNT walls on the real sample was

This article has been accepted for publication in a future issue of this journal, but has not been fully edited. Content may change prior to final publication. Citation information: DOI 10.1109/TCPMT.2019.2940511, IEEE Transactions on Components, Packaging and Manufacturing Technology

TABLE I
TOTAL AND EXTRACTED ONE CNT BUMP RESISTANCE OF THE GRAPHENE AND AU BRIDGE STRUCTURE WITH TWO CONFIGURATIONS OF CNT AREA

Configuration	W (mm)	L (mm)	CNT area			R_{total} (Ω)	R_{btm_Au} (Ω)	R_{top_Au} (Ω)	R_G (Ω)	$R_{Au-CNT-G}$ or $R_{Au-CNT-Au}$ (Ω)
			a (mm)	b (mm)	S (mm^2)					
A with graphene bridge (PET)	3.6	0.08	0.03	2.95	0.09	10.0	0.7	/	5.1	2.1
A with Au bridge (SiO_2/Si)	4.5	0.08	0.03	2.96	0.09	5.2	0.7	0.01	/	2.2
B with graphene bridge (SiO_2/Si)	4.2	0.77	0.28	0.28	0.08	128.1	7.0	/	110.7	5.2
B with Au bridge (SiO_2/Si)	3.4	0.61	0.30	0.30	0.09	18.2	7.0	0.12	/	5.5

estimated to be around 110 μm (details of the estimation can be found in Appendix A). The I_G/I_D peak ratio and average diameter of the CNTs was ~1.5 and ~3nm respectively as shown in Fig. 5. CNT density was estimated as ~10^{11} cm^{-2} (details of the density estimation are shown in Appendix B),

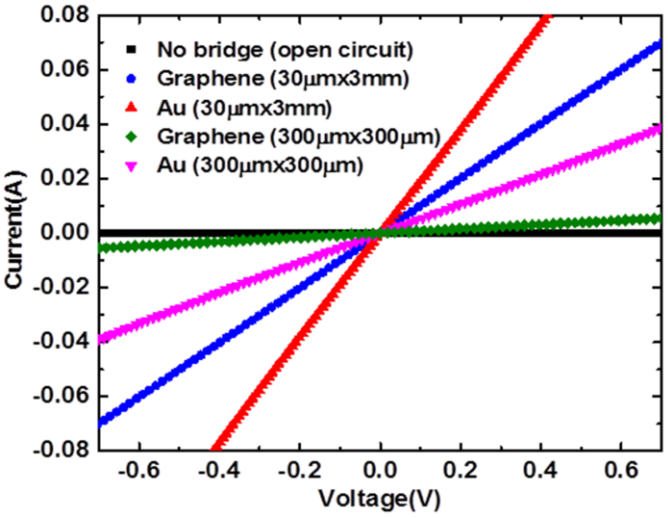

Fig. 6. 4pp I-V measurement results of the total resistance of the graphene and Au bridge structure with two configurations of CNT area.

which is expectedly to be much higher than PECVD grown CNTs ~10^9 cm^{-2} [38].

4PP I-V measurement is performed on the Au-CNT-graphene-CNT-Au structure with configuration A, as displayed in Fig. 6 (blue-dotted line). It is shown that the current increases linearly under the voltage sweep ranging from -1 to 1V. Short circuit between two CNT walls or bottom Au pads was excluded by I-V measurement before graphene transfer. After the transfer of graphene onto the CNTs, the gap between two CNT walls remained as shown in Fig. 4 (c) and (d), suggesting the omission of current shortage between two walls after the graphene transfer. Ruling out all possible shortages, it can be postulated that ohmic contact was achieved between the graphene and CNTs.

I-V curves of the graphene and Au bridge structure with two different CNT area configurations are shown in Fig. 6. The Au bridge structure shows a linear response to current upon voltage application, similar to its graphene bridge counterpart. However, its total resistance was smaller compared to the value of the graphene bridge structure with the same configuration of CNT area, possibly due to the significantly-large valued of R_G as compared to R_{top_Au}, as mentioned earlier. Meanwhile, for the graphene bridge structure, configuration A (30μm×3mm) with closer distance (L) between two CNT walls has much smaller total resistance than the value of configuration B (300μm × 300μm) as expected, due to the large R_G in the structure of configuration B.

This article has been accepted for publication in a future issue of this journal, but has not been fully edited. Content may change prior to final publication. Citation information: DOI 10.1109/TCPMT.2019.2940511, IEEE Transactions on Components, Packaging and Manufacturing Technology

The measured values of R_{btm_Au} and the estimated values of R_G and R_{top_Au} for various CNT-graphene configurations are listed in Table I. Detailed estimation method of R_G and R_{top_Au} is presented in the Appendix C. $R_{Au-CNT-G}$ and $R_{Au-CNT-Au}$ are extracted from (1) and (2) as shown in Table I. Under the same configuration, $R_{Au-CNT-G}$ has similar value with $R_{Au-CNT-Au}$ suggesting formation of similar ohmic contact was formed at the CNT/graphene interface, and at the CNT/top Au interface. The contact between CNTs and graphene can be possibly achieved by the Van der Waals forces as the current density ($\ll 10^8$ A/cm^2) induced from I-V measurements is relatively insignificant to fuse the CNTs and graphene with covalent carbon bonds [39]. On the other hand, the contact resistance between CNTs and graphene was slightly smaller than the contact resistance between CNTs and Au. A possible reason for this is the low discrepancy in the work functions of graphene/CNTs (4.6eV/4.7eV [40]), as compared to Au/CNTs (5.1eV/4.7eV), resulting in possible electron tunneling in CNT/graphene interface. Under identical CNT area,s the contact resistances between CNTs and graphene (or between CNTs and Au) of configuration A and B were different. This shows that a non-uniform current density exists at the CNT/graphene (or CNT/Au) contact due to the current crowding effect [41]. The effective contact area of configuration A is larger than configuration B resulting in smaller contact resistance in configuration A. The Ohmic contact obtained aligns well with the assumptions in using Eq. (1) and (2), as mentioned in the previous section. As Ohmic contact can be postulated, the contact resistance can be postulated to increase linearly with reduced contact area, as agreed by Ohm's law. In other words, a possible increase in contact resistance may be anticipated for miniaturized interconnects with smaller CNT-graphene contact area. However, in actual CNT-graphene interconnects, more uncertainties shall be considered, such as discrepancies in CNT height/crystallinity across CNTs, which requires further investigations to address these possible discrepancies.

The resistance of one CNT bump ($R_{Au-CNT-G}$) in this work is compared against the results from state-of-the-art as shown in Table II. By normalization of the CNT area, it shows the obtained outcomes from this work compares favourably with the state-of-the-art [35], [37]. However, as the reported studies used various CNT area dimensions, further study is needed to explore the possible factors affecting the CNT/graphene contact resistance with smaller CNT areas.

TABLE II
RESISTANCE OF ONE CNT BUMP (INCLUDING THE CNT/METAL (CNT/GRAPHENE) CONTACT RESISTANCE) OF THIS WORK AND THE REPORTED STATE-OF-THE-ART

	$R_{Au-CNT-Au}$ [35]	$R_{ZrN-CNT-Al}$ [37]	$R_{Au-CNT-Au}$ [6]	$R_{Au-CNT-G}$ (this work)
CNT bump resistance R (Ω)	280	457	16.1	2.1
CNT area (μm^2)	1963	2827	7854	90000
CNT height (μm)	120	300	132	110

Repeatability tests of the total resistance were conducted to each graphene and Au bridge structure as shown in Table III. Except for the graphene bridge structure with PET substrate, other three structures with SiO_2/Si substrate show increasing trend in resistances under the repeated voltage sweeps (-1V to 1V). This can be attributed to the damage of accumulating charges at the air gap between CNTs and graphene (or Au) contact. However, for the graphene bridge structure with PET substrate, the air gap can be shortened by the electrostatic force of accumulating charges after several voltage sweeps since the PET substrate is flexible. Thus, the total resistance of graphene bridge structure with PET substrate decreases initially, and then stabilized with the voltage sweeps repeated.

IV. CONCLUSION

In this work, transfer process of a top graphene layer onto the as-grown CNT bundles was successfully performed. Direct graphene-to-CNT contact was formed at the CNT/graphene interface. 4PP I-V characterization suggests that ohmic contact was formed between the graphene and CNTs. Low CNT bump resistance of 2.1Ω for 90,000 μm^2 CNT area including the CNT/graphene contact resistance was obtained, demonstrating reduction of contact resistance between CNT and Au under the same fabrication and measurement conditions. This work presents the preliminary results for the assembly process of top-transferred graphene on CNTs and the electrical properties of the direct CNT/graphene contact. For the future work, the reduced contact resistance enables scaling down of CNT-graphene interconnects from the investigated 90,000 μm^2 CNT area with improved electrical properties for further exploration, and bottom Au pads of the bridge structure shall be replaced by the patterned graphene to complete the full-carbon 3D interconnection.

TABLE III
REPEATABILITY TESTS OF THE TOTAL RESISTANCE FOR THE GRAPHENE AND AU BRIDGE STRUCTURE

Sample	R_{total} (Ω)				
	1st	2nd	3rd	4th	5th
A with graphene bridge (PET)	11.1	10.6	**10.0**	10.2	10.0
A with Au bridge (SiO_2/Si)	**5.2**	6.2	7.0	6.8	7.0
B with graphene bridge (SiO_2/Si)	**128.1**	135.4	135.0	135.0	133.7
B with Au bridge (SiO_2/Si)	**18.2**	21.3	21.8	22.3	23.3

This article has been accepted for publication in a future issue of this journal, but has not been fully edited. Content may change prior to final publication. Citation information: DOI 10.1109/TCPMT.2019.2940511, IEEE Transactions on Components, Packaging and Manufacturing Technology

APPENDIX

A. *Estimation of the CNTs vertical length*

The vertical length of CNT walls on the dummy sample was measured directly from the cross-sectional SEM image as shown in Fig. A1 (a). The planar length of CNT walls on the same dummy sample measured from the tilted-view SEM image tilted was shown in Fig. A1 (b). From the tilted-view SEM image, the planar length of CNT walls on the real sample was measured as shown in Fig. A2 with satisfactory uniformity. Using the same ratio of the planar and vertical length of CNTs on the dummy sample, the vertical length of CNT walls on the real sample can be calculated to be 110 μm.

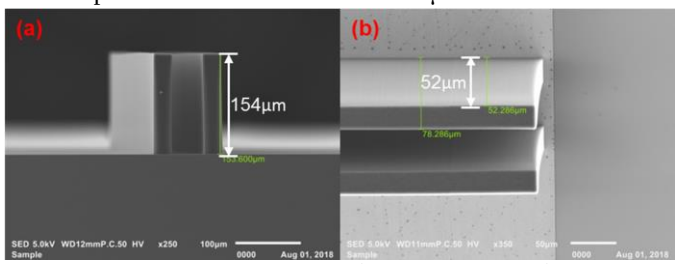

Fig. A1. (a) Cross-section SEM image of the vertical length of CNT walls on the dummy sample and (b) the planar length of CNT walls on the same dummy sample from the top-view SEM image tilted at 20˚.

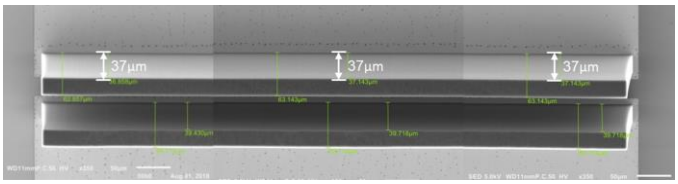

Fig. A2. The planar length of CNT walls on the real sample from the top-view SEM image tilted at 20˚.

B. *CNT density estimation*

The average diameter of CNTs was ~3nm as shown in TEM images. Using the formula below, the densities of CNTs (ρ) can be estimated:

$\rho = \frac{F \times S}{\pi(d/2)^2}$, where F is the filling factor ratio (surface area covered with CNTs after densification/surface area covered with CNTs before densification), S is the surface area before densification, d is the average diameter of CNTs. To determine the filling ratio, bumps of 1 mm^2 were patterned (not shown) on each sample and subjected to same growth process. The densification process was performed by immersing the sample in IPA. The filling factor was calculated to be 0.132 ± 0.008 by using imaging software pixel calculation, based on more than 10 CNT bumps. Using the abovementioned technique, the surface density of CNTs was calculated to be ~10^{11} cm^{-2}.

C. *Determination of W_{eff} and estimation of R_G and R_{top_Au}*

R_G and R_{top_Au} can be estimated using (3): $R = \frac{L}{W_{eff}} R_S$, where L is the distance between two CNT bundles; W_{eff} is the effective width of top graphene layer or Au film; R_S is the sheet resistance of the graphene layer or Au film. Based on two configurations of CNT area and the physical width (W) of the graphene layer or Au film, as shown in Fig. 3 and Table I, it can be postulated that:

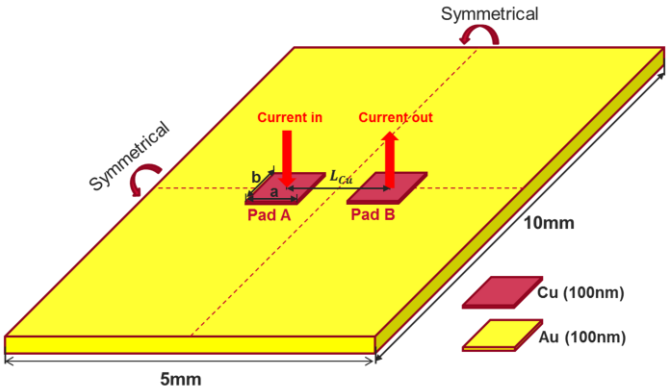

Fig. A3. Illustration of two Cu electrodes replacing the two CNT bundles on the top of Au film.

1) For the CNT area with configuration A, $W_{eff} \approx$ W since the width b of CNT area (3mm) is close to W (3.6 or 4.5mm) and the L (80μm) is much smaller compared to the value of b (3mm);
2) For the CNT area with configuration B, $W_{eff} <$ W since the width b of CNT area (300μm) is much smaller than W (4.2 or 3.4mm) and the L (770 or 610μm) is larger than the value of b (300μm).

TABLE I (Appendix)
4PP I-V MEASURED TOTAL RESISTANCES OF DIFFERENT L_{Cu} FROM THREE BATCHES OF SAMPLES

L_{Cu} (mm)	Resistance (mΩ)		
	Batch 1	Batch 2	Batch 3
0.396	104	113	113
0.594	154	156	152
0.794	186	190	193

For CNT area with configuration B, W_{eff} can be determined by transfer length method (TLM) with two Cu electrodes replacing the two CNT bundles on the top of Au film with sample size of 5mm × 10mm, as shown in Fig. A3. The total resistance between two Cu electrodes can be expressed as $R_{total} = 2(R_{Cu/Au} + R_{Cu}) + \frac{R_S}{W_{eff}} L_{Cu}$, where $R_{Cu/Au}$ and R_{Cu} are the contact resistance between Cu and Au and the bulk resistance of one Cu electrode, respectively; R_S is the sheet resistance of Au film; L_{Cu} is the distance between two Cu electrodes. By varying the distance between two Cu electrodes, the total resistance vs. L_{Cu} will have a linear response. The slope equals to R_S/W_{eff}.

Fig. A4 shows the optical images of patterned two Cu electrodes on the Au film with three different values of L_{Cu}. Table I (Appendix) shows the 4PP I-V measured total resistances of different L_{Cu} from three batches of samples. Fig. A5 plots the linear response of the total resistance vs. L_{Cu} with a slope 194.3 mΩ/mm. R_S of Au film was measured to be 313 mΩ by 4PP sheet resistance measurement machine. Subsequently, W_{eff} was calculated to be 1.6 mm (applicable for L within the range of 396-794 μm).

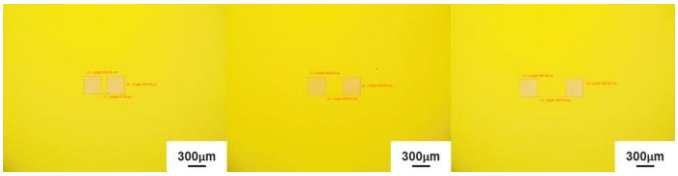

Fig. A4. Optical images of patterned two Cu electrodes on the Au film with three different values of L_{Cu}.

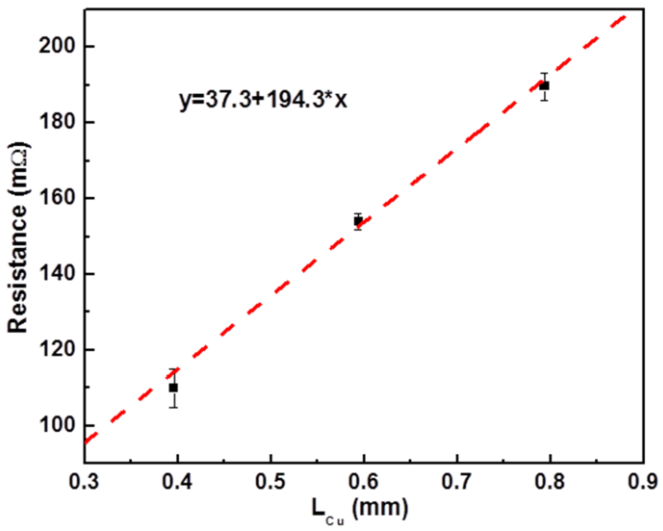

Fig. A5. The linear response of the total resistance vs. L_{Cu}.

ACKNOWLEDGMENT

Authors are grateful to the support and resources from Centre for Micro-/Nano-electronics (NOVITAS), CNRS International NTU THALES Research Alliance (CINTRA) and Silicon Technologies Center of Excellence (Si-COE) at NTU, Singapore. Authors also thank the support from management and staff in Nanyang Nano Fabrication Centre (N2FC) at NTU, Singapore.

REFERENCES

[1] R. R. Schaller, "MOORE ' S LAW : past , present , future," *IEEE Spectr.*, vol. 34, no. 6, pp. 52–59, 1997.

[2] W. Arden, M. Brillouët, P. Cogez, M. Graef, B. Huizing, and R. Mahnkopf, "ITRS: More-than-Moore," *Int. Technol. Roadmap Semicond.*, 2010.

[3] R. R. Tummala, "Moore's Law meets its match," *IEEE Spectr.*, vol. 43, no. 6, pp. 44–49, 2006.

[4] P. G. Emma and E. Kursun, "Is 3D chip technology the next growth engine for performance improvement?," *IBM J. Res. Dev.*, vol. 52, no. 6, pp. 541–552, 2010.

[5] N. Khan *et al.*, "3-D packaging with through-silicon via (TSV) for electrical and fluidic interconnections," *IEEE Trans. Components, Packag. Manuf. Technol.*, vol. 3, no. 2, pp. 221–228, 2013.

[6] T. Wang, K. Jeppson, L. Ye, and J. Liu, "Carbon-nanotube through-silicon via interconnects for three-dimensional integration," *Small*, vol. 7, no. 16, pp. 2313–2317, 2011.

[7] H. Tong, "Microelectronics packaging present and future," *Mater. Chem. Phys.*, vol. 40, pp. 147–161, 1995.

[8] J. H. Lau, "Overview and outlook of through-silicon via (TSV) and 3D integrations," *Microelectron. Int.*, vol. 28, no. 2, pp. 8–22, 2011.

[9] Y. Zhu, J. Zhang, H. Y. Li, C. S. Tan, and G. Xia, "Study of near-surface stresses in silicon around through-silicon vias at elevated temperatures by Raman spectroscopy and simulations," *IEEE Trans. Device Mater. Reliab.*, vol. 15, no. 2, pp. 142–148, 2015.

[10] I. De Wolf, K. Croes, and E. Beyne, "Expected Failures in 3-D Technology and Related Failure Analysis Challenges," *IEEE Trans. Components, Packag. Manuf. Technol.*, vol. 8, no. 5, pp. 711–718, 2018.

[11] W. S. Zhao *et al.*, "High-Frequency Modeling of On-Chip Coupled Carbon Nanotube Interconnects for Millimeter-Wave Applications," *IEEE Trans. Components, Packag. Manuf. Technol.*, vol. 6, no. 8, pp. 1226–1232, 2016.

[12] A. Maffucci, F. Micciulla, A. E. Cataldo, G. Miano, and S. Bellucci, "Modeling, Fabrication, and Characterization of Large Carbon Nanotube Interconnects with Negative Temperature Coefficient of the Resistance," *IEEE Trans. Components, Packag. Manuf. Technol.*, vol. 7, no. 4, pp. 485–493, 2017.

[13] T. Wang *et al.*, "Through-silicon vias filled with densified and transferred carbon nanotube forests," *IEEE Electron Device Lett.*, vol. 33, no. 3, pp. 420–422, 2012.

[14] H. J. Dai, E. W. Wong, and C. M. Lieber, "Probing Electrical Transport in Nanomaterials: Conductivity of Individual Carbon Nanotubes," *Science (80-.).*, vol. 272, no. 5261, pp. 523–526, 1996.

[15] T. Xu, Z. Wang, J. Miao, X. Chen, and C. M. Tan, "Aligned carbon nanotubes for through-wafer interconnects," *Appl. Phys. Lett.*, vol. 91, no. 4, pp. 79–82, 2007.

[16] B. Q. Wei, R. Vajtai, and P. M. Ajayan, "Reliability and current carrying capacity of carbon nanotubes," *Appl. Phys. Lett.*, vol. 79, no. 8, pp. 1172–1174, 2001.

[17] P. Kim, L. Shi, A. Majumdar, and P. L. McEuen, "Thermal transport measurements of individual multiwalled nanotubes," *Phys. Rev. Lett.*, vol. 87, no. 21, pp. 215502-1-215502–4, 2001.

[18] T. Y. Choi, D. Poulikakos, J. Tharian, and U. Sennhauser, "Measurement of thermal conductivity of individual multiwalled carbon nanotubes by the 3-ω method," *Appl. Phys. Lett.*, vol. 87, no. 1, pp. 1–3, 2005.

[19] Q. Kong *et al.*, "Thermal conductivity characterization of three dimensional carbon nanotube network using freestanding sensor-based 3ω technique," *Surf. Coatings Technol.*, vol. 345, no. March, pp. 105–112, 2018.

[20] Q. Kong *et al.*, "Novel three-dimensional carbon nanotube networks as high performance thermal interface materials," *Carbon N. Y.*, vol. 132, pp. 359–369, 2018.

[21] J. W. Jiang, J. S. Wang, and B. Li, "Thermal expansion in single-walled carbon nanotubes and graphene: Nonequilibrium Green's function approach," *Phys. Rev. B - Condens. Matter Mater. Phys.*, vol. 80, no. 20, pp. 1–7, 2009.

[22] J. Vanpaemel *et al.*, "Growth and integration challenges for carbon nanotube interconnects," *Microelectron. Eng.*, vol. 120, pp. 188–193, 2014.

[23] S. Vollebregt, R. Ishihara, F. Tichelaar, J. Van Der Cingel, and K. Beenakker, "Electrical characterization of carbon nanotube vertical interconnects with different lengths and widths," *2012 IEEE Int. Interconnect Technol. Conf. IITC 2012*, pp. 1–3, 2012.

[24] I. Soga *et al.*, "Carbon nanotube bumps for LSI interconnect," *Proc. - Electron. Components Technol. Conf.*, pp. 1390–1394, 2008.

[25] T. Iwai, H. Shioya, D. Kondo, S. Hirose, and A. Kawabata, "Thermal and source bumps utilizing carbon nanotubes for flip-chip high power amplifiers," in *IEEE International Electron Devices Meeting*, 2005, pp. 257–260.

[26] S. Hermann, B. Pahl, R. Ecke, S. E. Schulz, and T. Gessner, "Carbon nanotubes for nanoscale low temperature flip chip connections," *Microelectron. Eng.*, vol. 87, no. 3, pp. 438–442, 2010.

[27] C. Xu, H. Li, and K. Banerjee, "Modeling, analysis, and design of graphene nano-ribbon interconnects," *IEEE Trans. Electron Devices*, vol. 56, no. 8, pp. 1567–1578, 2009.

[28] H. Li, C. Xu, N. Srivastava, and K. Banerjee, "Carbon Nanomaterials for Next-Generation Interconnects and Passives: Physics, Status, and Prospects," *IEEE Trans. Electron Devices*, vol. 56, no. 9, pp. 1799–1821, 2009.

[29] D. Sarkar, C. Xu, H. Li, and K. Banerjee, "High-frequency behavior of graphene-based interconnects-Part I: Impedance modeling," *IEEE Trans. Electron Devices*, vol. 58, no. 3, pp. 843–852, 2011.

[30] D. Sarkar, C. Xu, H. Li, and K. Banerjee, "High-frequency behavior of graphene-based interconnect-sPart II: Impedance analysis and implications for inductor design," *IEEE Trans. Electron Devices*, vol. 58, no. 3, pp. 853–859, 2011.

[31] W. S. Zhao, Y. F. Liu, Z. Yong, Y. Fang, and W. Y. Yin, "Modeling

and characterization of carbon-based heterogeneous interconnects for 3-D ICs," *EDAPS 2013 - 2013 IEEE Electr. Des. Adv. Packag. Syst. Symp.*, pp. 154–157, 2013.

[32] J. Jiang, J. Kang, J. H. Chu, and K. Banerjee, "All-Carbon Interconnect Scheme Integrating," in *International Electron Devices Meeting*, 2017, pp. 342–345.

[33] K. Ghosh, N. Ranjan, Y. K. Verma, and C. S. Tan, "Graphene-CNT hetero-structure for next generation interconnects," *RSC Adv.*, vol. 6, no. 58, pp. 53054–53061, 2016.

[34] N. Chiodarelli *et al.*, "Integration of Vertical Carbon Nanotube Bundles for Interconnects," *J. Electrochem. Soc.*, vol. 157, no. 10, p. K211, 2010.

[35] T. Wang, K. Jeppson, N. Olofsson, E. E. B. Campbell, and J. Liu, "Through silicon vias filled with planarized carbon nanotube bundles," *Nanotechnology*, vol. 20, no. 48, 2009.

[36] S. C. Lim *et al.*, "Contact resistance between metal and carbon nanotube interconnects: Effect of work function and wettability," *Appl. Phys. Lett.*, vol. 95, no. 26, pp. 93–96, 2009.

[37] S. Vollebregt, S. Banerjee, F. D. Tichelaar, and R. Ishihara, "Carbon nanotubes TSV grown on an electrically conductive ZrN support layer," *2015 IEEE Int. Interconnect Technol. Conf. 2015 IEEE Mater. Adv. Met. Conf. IITC/MAM 2015*, pp. 281–283, 2015.

[38] C. C. Yap, "DEVELOPMENT OF CARBON NANOTUBES FOR INTERCONNECTS AND NANO-PACKAGING APPLICATIONS," Nanyang Technological University, 2013.

[39] K. Asaka, M. Karita, and Y. Saito, "Modification of interface structure and contact resistance between a carbon nanotube and a gold electrode by local melting," *Appl. Surf. Sci.*, vol. 257, no. 7, pp. 2850–2853, 2011.

[40] P. Liu *et al.*, "Measuring the work function of carbon nanotubes with thermionic method," *Nano Lett.*, vol. 8, no. 2, pp. 647–651, 2008.

[41] S. M. Song and B. J. Cho, "Contact resistance in graphene channel transistors," *Carbon Lett.*, vol. 14, no. 3, pp. 162–170, 2013.

Ye Zhu received her B.S. in Chemistry from Xiamen University, China, in 2012. After that, she went to the Department of Materials Engineering at the University of British Columbia, Canada, and graduated with master degree in 2015. Her master's project was mainly about the stress analysis of through silicon via (TSV) in three-dimensional integration circuits (3-D ICs) by micro-Raman spectroscopy and FEA simulations. She is currently pursuing her Ph.D. degree in the School of Electrical and Electronic Engineering, Nanyang Technological University, Singapore. Her Ph.D. project mainly focuses on the implementation of full carbon-based 3-D interconnects.

Chong Wei Tan received his B. Eng. in Electrical and Electronics Engineering (EEE) from Nanyang Technological University (NTU), Singapore, in 2005. After that, he received his M. Eng. in Mechanical Aerospace Engineering from NTU in 2007, and PhD in EEE from NTU in 2015. He is currently holding a postdoctoral research fellow position in School of Electrical and Electronic Engineering at NTU. His current research interests include carbon-based hybrid materials for MEMS and nano-electronics applications, thermal management in electronic devices, advanced 3D interconnect TSV, diamond as substrate for high power devices, and carbon nanotubes for field emission and RF applications, etc.

Shen Lin Chua received the B. Eng. in Mechanical and Aerospace Engineering from Nanyang Technological University (NTU), Singapore in 2012. From year 2013 to 2016, he held a Research Assistant position in Termasek Laboratories@NTU, School of Electrical and Electronics Engineering (EEE), NTU. From year 2017 to 2019, he held a Project Officer position in Centre of Micro-/Nano-electronics (NOVITAS) in School of EEE, NTU. Currently, he is doing his PhD in EEE and holding a Project Officer position in Termasek Laboratories@NTU, Microsystems Technology Development Centre. His research interest include material bonding for 3D integration, electronics packaging, wafer-to-wafer bonding, and thin film technologies for CMOS-compatible novel electronic devices.

Yu Dian Lim received the B. Eng. in Materials and M. Sc. of Materials Engineering from University of Malaya (UM), Malaysia, in 2011 and 2014, respectively. After that, he received the PhD in EEE from Nanyang Technological University (NTU), Singapore in 2018. He is currently holding a postdoctoral research fellow position in School of Electrical and Electronic Engineering, NTU. He has involved in multidisciplinary researches, including nanomaterials, nano-electronics, MEMS fabrication, communication device design etc. His current research interests include silicon photonics integrated circuit design, quantum computing devices, and tribo-electric nano-generator (TENG) design and application.

Boris Vaisband is currently a postdoctoral scholar at the University of California, Los Angeles, working on wafer level heterogeneous systems integration. He received a B.S. degree in Computer Engineering from the Technion – Israel Institute of Technology, Haifa, Israel in 2011, and a M.S. and Ph.D. degrees in Electrical Engineering from the University of Rochester, Rochester, NY, respectively, in 2012 and 2017. His current research interests include integration of heterogeneous systems, communication, power delivery, global interconnects, and thermal aware design and floor planning.

Beng Kang Tay is currently a Professor in School of Electrical and Electronics Engineering (EEE), Nanyang Technological University (NTU), Singapore. He is also the Deputy Director for CNRS-International-NTU-Thales Research Alliance (CINTRA). He

received his Bachelor (Hons) degree from National University of Singapore in 1985 and Ph.D. from Nanyang Technological University, Singapore in 1999. His current research is includes growth and application of carbon based and 2D materials for thermal and high frequency applications.

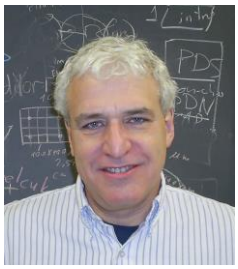

Eby G. Friedman received the B. S. degree from Lafayette College, Easton, Pennsylvania in 1979, and the M. S. and Ph. D. degrees from the University of California, Irvine, in 1981 and 1989, respectively, all in electrical engineering. Dr. Friedman has been with the Department of Electrical and Computer Engineering at the University of Rochester, Rochester, New York, since 1991, where he is a Distinguished Professor and Director of the High Performance VLSI/IC Design and Analysis Laboratory. He is a Fellow of the IEEE, Chair of the steering committee for the IEEE Transactions on VLSI Systems, a Regional Editor of the Journal of Circuits, Systems and Computers, a Member of the editorial board of the Analog Integrated Circuits and Signal Processing, Microelectronics Journal, Journal of Low Power Electronics, and Journal of VLSI Signal Processing.

Chuan Seng Tan received his B.Eng. degree in electrical engineering from University of Malaya, Malaysia, in 1999. Subsequently, he completed his M.Eng. in advanced materials from the National University of Singapore in year 2001. After that, he is conferred PhD in electrical engineering from Massachusetts Institute of Technology, Cambridge, USA in year 2006. He is currently an Associate Professor in School of Electrical and Electronics Engineering (EEE), Nanyang Technological University (NTU), Singapore. At the same time, he is also the Associate Dean (Academic) in College of Engineering, NTU. His research interests are semiconductor process technology and device physics. He provides his service as committee member for International Conference on Wafer Bonding, IEEE-3DIC, IEEE-EPTC, IEEE-ECTC, IEEE-EDTM, IEEE-GFP and ECS-Wafer Bonding. He is an associate editor for Elsevier Microelectronics Journal (MEJ) and IEEE Transactions on Components, Packaging and Manufacturing Technology. He is a senior member of IEEE and a recipient of the 2019 Exceptional Technical Achievement Award from the IEEE Electronics Packaging Society.